Swarthmore College
Works

Senior Theses, Projects, and Awards | Student Scholarship

2021

How about that extension? Biomechanical roles of spines in crustacean nauplii

Emily N. Branam , '21

Follow this and additional works at: https://works.swarthmore.edu/theses

Part of the Biology Commons

Recommended Citation

Branam, Emily N. , '21, "How about that extension? Biomechanical roles of spines in crustacean nauplii" (2021). *Senior Theses, Projects, and Awards*. 164.
https://works.swarthmore.edu/theses/164

Please note: the theses in this collection are undergraduate senior theses completed by senior undergraduate students who have received a bachelor's degree.
This work is brought to you for free by Swarthmore College Libraries' Works. It has been accepted for inclusion in Senior Theses, Projects, and Awards by an authorized administrator of Works. For more information, please contact myworks@swarthmore.edu.

How about that extension?:

Biomechanical roles of spines in crustacean nauplii

By

Emily Nicole Branam

Swarthmore College

Advisor:

Kit Yu Karen Chan, Assistant Professor

Biology, Swarthmore College

A thesis submitted to the Biology Department

in partial fulfillment of the requirement of the Honors Program

How about that extension?:
Biomechanical roles of spines in crustacean nauplii

Abstract

Marine plankton possess elongated body structures, such as spines and horns, that increase drag on the body. While these extensions are often considered an anti-predation mechanism, the biomechanical implications of these structures are less studied. Using the barnacle nauplii *Octolasmis spp.*, I explore the role of one such body extension, the dorsal thoracic spine, through amputation. Motion analysis revealed slower swimming and more erratic trajectories in dorsal thoracic spine amputees than those in control. Limb kinematic adjustments such as a larger beat amplitude, increased phase lag, and reduced contralateral symmetry were observed in amputees. While these changes may act to partially compensate for the loss of the spine by increasing propulsion and streamlining flow, they were unable to fully restore swimming proficiency. Further Particle Image Velocimetry (PIV) on live nauplii revealed increased predation risk by rheotactic predators as well as reduced feeding in amputees due to increased relative area of influence and decreased flux. A dynamically scaled model of spine loss supported area of influence results observed in live nauplii. The interaction between body extensions and limb motion shape swimming performance in nauplii, and in turn, shapes the evolution of naupliar form.

Note:
Part of the information presented in this thesis is published in the journal of Integrative and Comparative Biology (Branam et al., 2021).

Introduction

Body extensions, such as spines, horns, and setae, are common among marine plankton (Martin *et al.* 2014). It has been suggested that these structures serve anti-predatory roles, specifically, escaping size-limited predators through increase in body length (Schlüter *et al.* 1987; Padisák *et al.* 2003; Herzog *et al.* 2016). The additional form drag these body extensions create can also help prevent sinking and increase stability in a given orientation (Walsby & Xypolyta 1977; Padisák *et al.* 2003). However, it is possible that these features experienced selective pressure related to other ecological functions. For instance, the presence or absence of long body extensions was linked to trophic

mode (Wong *et al.* 2020a). To determine the potential roles these extensions play, in this thesis, I explore the biomechanical role of one type of body extension in the highly conserved Crustacean naupliar form.

Crustacean larvae make up a large proportion of planktonic biomass, and they act as important grazers and prey for higher trophic levels (Turner *et al.* 2001; Vargas *et al.* 2006; Chew *et al.* 2012). Crustacean larvae have varied morphology but stick to a highly conserved basic form, the nauplius (Dahms 2000). The three sets of swimming appendages known as the antennules, antennae, and mandibles are common to all naupliar forms, while the types of body extensions they possess are more variable, e.g. the caudal rami in copepods or frontal horns and dorsal thoracic spine (dts) in barnacles (Williams 1994; Martin *et al.* 2014). Exploring how these morphological features impact function can allow better understanding of this form's evolution.

Nauplii range in size from 100 to 1000 μm and swim at speeds between 0.1 to10 mm s^{-1}. Therefore, they operate in low to intermediate Reynolds number (*Re*) environments, where viscous forces dominate (Purcell 1977; Wong *et al.* 2018). As demonstrated by the scallop theorem, a swimmer that utilizes reciprocal motion, or time symmetric motion, is unable to achieve net forward displacement in low *Re* environments (Purcell 1977). Instead, multilegged crustacean nauplii achieve net forward displacement with a tail to head metachronal wave, deemed the "biomechanically optimal stroke pattern" in these environments (Murphy *et al.* 2011; Zhang *et al.* 2014; Takagi 2015; Hayashi & Takagi 2020). This metachronal stroke pattern can be complemented by adjusting the effective area used in propulsion by fanning out setae on the tips of appendages during the power stroke and collapsing these setae into bundles during the

recovery stroke to break the confines of reciprocal motion (Koehl 1998; Lamont & Emlet 2018; Von Dassow & Emlet 2020). Wong *et al.* (2020a) further suggested that these non-collapsible body extensions, i.e. spines and horns, add to the overall surface area and could act as a functional tether to increase drag during swimming.

For multilegged crustacean nauplii, swimming is also impacted by limb kinematics. For instance, an increase in pleopod beat frequency allowed krill to achieve higher speeds (Swadling *et al.* 2005). Increases in stroke amplitude, or the angular sweep of an appendage, can also increase net forward displacement (Murphy *et al.* 2011; Lenz *et al.* 2015). Distinct behaviors, such as hovering and fast forward swimming in krill, can be produced by changes in coordinated limb movement including phase lag (Ford & Santhanakrishnan 2020). Body rotation over multiple axes can also be achieved via variation in limb kinematics: pronation, supination, and contralateral asymmetry in limb beat (asynchrony in the beat patterns of one pair of appendages) (Niimoto *et al.* 2020). The flexible limbs, such as the ones possessed by mysids, krill, branchiopod, and other crustacean nauplii can be flexed during the recovery stroke to reduce drag (Hessler 1985; Johnson & Tarling 2008). These flexible propulsors share an optimal bending range which is highly conserved across taxa from small plankton to large mammals (Lucas *et al.* 2014). While limb kinematics alone can greatly impact swimming, interaction between limb kinematics and body extensions, such as spines and horns, has not yet been addressed and likely complicates swimming performance further.

Many ecological functions of crustacean nauplii are reliant on the way that fluid flows around the body, which is strongly influenced by limb kinematics. For instance, in free swimming copepods, the hovering behavior creates a wide and conic flow geometry

while upward swimming or sinking behaviors form long and narrow flow geometries (Jiang *et al.* 2002a; Jiang *et al.* 2002b). Presence of body extensions also impact fluid flow. Body extensions can increase cross sectional area of the organism, consequently increasing drag (Vogel 1988). The increased drag effectively tether the organisms (Emlet *et al.* 1985; Wong *et al.* 2018; Wong *et al.* 2020a). Shape and direction of fluid flow play important roles in numerous ecologic functions such as feeding, avoiding predation, advertisement of presence to potential mates, etc. (Strickler 1998; Kiørboe *et al.* 2010; Jiang & Kiørboe 2011). In barnacle nauplii, suspension feeding relies on a feeding current generated during swimming to direct the flow of food laden water to the feeding area underneath the labrum (Lochhead 1936; Rainbow & Walker 1976). Additionally, many nauplii are under threat of predation by rheotactic predators, and as such, predator avoidance relies on the minimization of hydrodynamic signal while swimming (Kiørboe *et al.* 2010; Kiørboe *et al.* 2014). Thus, the effects of adjustments to limb kinematics and the interaction between body extensions and limb movement not only influence swimming performance but also overall fitness and survival.

Despite the strongly conserved naupliar form of crustaceans, there are large interspecific variations, making it a useful case study in exploring the role of body extensions (Martin *et al.* 2014; Wong *et al.* 2018). Specifically, *Lepadidae* and *Poecilasmatidae* families of barnacles possess comparatively long dorsal thoracic spines and frontal horns to other barnacle families (Wong *et al.* 2018). The extreme morphology of the epibiotic *Octolasmis spp.* (within *Poecilasmatidae*), a genus that possess narrow head shields and long narrow body extensions, make it a suitable model organism to determine the dts's role in swimming.

To quantify the role of the dts in swimming and fluid disturbance, I used video motion analysis, limb tracking, and Particle Image Velocimetry to compare kinematics and hydrodynamics of freely swimming nauplii with their dts intact and amputated. Amputation experiments provide useful insight into how removal of these structures influences locomotion (Delcomyn 1991; Zhang *et al.* 2015). In addition to observing live individuals, I also employed physical models to explore parameter spaces not occupied by real-life organisms, in which individual structures, e.g., limbs, spines, horns, could be selectively attached or removed (Vogel 1981; Koehl 2003). Specifically, with dynamically scaled models, I matched *Re* number such that observations on the physical model could be translated to real organisms (Loudon *et al.* 1994). Limbless models can be used to examine the contribution of morphology to drag and eliminate potential contributions of swimming kinematics (Gutarra *et al.* 2019). Through separation of limb kinematics and morphology, a limbless dynamically scaled model acts as a useful mechanism in defining the specific contributions of body extensions to ecologically relevant fluid flow and hydrodynamic disturbance. Using these approaches, the overall goal of this thesis is to determine the role of body extensions in the swimming of crustacean nauplii through a case study on the dts in *Octolasmis spp*. nauplii.

Materials and methods

Adult collection and larval culturing

To obtain adult *Octolasmis spp.,* the crab *Portunus sanguinolentus* was purchased from a wet market in Keelung, Taiwan. Adult *O. cor* were then cut from the gills, while

O. warwickii was removed from the carapace and kept in 0.45 μm filtered seawater (FSW). Adults were fed with newly hatched *Artemia sp. ad libitum* until larvae were released. Released stage II larvae were transferred to FSW at 34 psu and kept at room temperature (~25°C) and randomly divided into two treatment groups, control and amputated (Fig.1). Using a custom-made ultra-fine needle and micro-scalpel composed from tungsten wire and glass pipette, 50% of the dts was removed lengthwise from the amputee treatment group following the methods in Wong *et al.* (2020a). Because nauplii were small and not given an anesthetic (to minimize potential influences on behavior), manipulating the nauplii was challenging. Therefore, only 50% of the dts was removed since it was a substantial portion relative to *Octolasmis*'s long spines but was short enough to avoid potential damage to the anus or the abdominal process. Control group larvae were similarly manipulated but not cut to account for effects of handling.

Population scale observations on free swimming nauplii

Stage II *O. cor* nauplii were placed in 25 mL cell culture flasks filled with 34 psu FSW. The temperature was regulated by a recirculating water bath kept at 25°C. The setup was lit with 850 nm infrared light and was filmed at 20 fps with an industrial camera (GS132, Vezutech, Ltd.) fitted with a 35-80 mm zoom lens at 1280x1024 pixel resolution. Four replicate videos were taken for each treatment, each using new nauplii. The nauplii was filmed for 6-7 minutes per replicate. Videos were imported into FOSICA (Wallingford Imaging Ltd.) to mask tank edges and subtract the backgrounds for each video. Path tracking was then performed with the in-house Matlab program Tracker3D. Frame rate noise was removed, and the overall direction of travel was determined from

the resulting trajectories by applying smoothing splines. The following metrics were computed for each path: 1) path duration, 2) gross speed (the first derivative of the smoothing spline), 3) net speed (the straight-line distance between start and end of a path divided by path duration), 4) net horizontal velocity ($U_{free\ swim}$), 5) net vertical velocity ($V_{free\ swim}$), 6) number of crossings across a mid-line approximating smoothing spline, 7) and average crossing distance. A "crossing" was defined as the point at which an individual path transected its respective midline approximating smoothing spline (Fig. 2).

Individual scale observations on free swimming nauplii

Setup for high speed videography followed Chan *et al.* (2013) and Gemmell *et al.* (2014). *O. warwickii* nauplii were recorded in a 25 x 75 x 5 mm glass cuvette with a FastCam Mini UX100 (Photron Ltd.) fitted with a bellows and a 60mm focal length lens at 2000 frames s^{-1} at 1280 x 1024 pixels (Wong *et al.* 2020a). Larvae were placed in a dark room and kept at 25°C using a larger 400 mL buffer tank. For fluid flow tracing, cuvettes were seeded with *Isochrysis galbana* (*T-iso*). Thirty individuals were used for each video session, and only dorsal/ventral view (xy plane) videos were analyzed. Sample size is reliant on freely swimming individuals entering the <2 mm^2 field of view. Therefore, only a subset of these individuals were used for further analysis.

Larval limb tracking

A full stroke cycle of larval limb positions for both left and right sides were tracked for each individual at every 20th frame extracted from high-speed video.

Beginning of the power stroke was defined as the time point in which the antennae were most rostrally-extended. The beginning of the recovery stroke was defined as the time point in which the antennae were the most caudally-extended. The tip of each appendage (antennule, antennae, and mandible) was defined as the point at which the appendage ended and setae began. To track limb position, limb tips were landmarked with tpsDIG2 (version 2.31). To track limb position in relation to the body, a body centroid was calculated from three body landmarks – the tip of the left horn, right horn, and dorsal thoracic spine. Due to amputation, the dts landmark was placed at the point at which the spine was cut in amputees, reflecting a potential shift in the center of mass (Fig. 1). Some larvae were excluded from limb kinematic analysis due to morphological abnormalities such as a bent tail or horns as well as build-up of algae on the body. In all, ten amputated nauplii videos and nine control nauplii videos were compared.

Limb beat angle θ of a given appendage was the angle between the vector $\overrightarrow{CA}$ (centroid to appendage tip) and $\overrightarrow{CT}$ (centroid to dts tip). Angular separation between limb pairs was calculated as a proxy for phase lag at four time points: start of power stroke, mid power stroke, end of power stroke/start of recovery stroke, and mid recovery stroke. Time points were determined based on limb beat angle of the right antennae because this pair of limbs was the major contributor to propulsion (Wong *et al.* 2020a). Contralateral symmetry in limb beats was tested by subtracting limb beat angle of the right appendage from the left for each pair of appendages. Overall movement of each individual during a stroke cycle was characterized by net displacement normalized by body length and the forward to backward displacement ratio (a measure of movement efficiency). Limb beat frequency was calculated based on the stroke duration.

Limb flexion is known to be highly conserved across taxa working within intermediate and high *Re* environments (*Re* ranges from ~40 to ~10^7). In order to compare this trend to low *Re* swimmers, I tracked the flexion point and flexion ratio of the antennae across stroke cycle similarly to Lucas *et al.* (2014). Flexion point was defined as the antenna's point of maximum curvature (Fig. 1). The tip of the appendage was marked as the flexion point when the antenna was fully extended and straight. The angle of flexion (φ) was then calculated as the dot product of the vectors from the flexion point to the body centroid $\overrightarrow{CI}$ and from the flexion point to antenna tip $\overrightarrow{CP}$. The inflection ratio was the $|\overrightarrow{CI}|$ divided by the sum of $|\overrightarrow{CI}|$ and $|\overrightarrow{CP}|$.

Flow field analysis

Particle image velocimetry analysis follows Wong *et al.* (2020a). Velocity vector fields were visualized for each nauplius. Each nauplius was algorithmically masked using a combination of smoothing, sliding maximum, and sliding minimum subtraction parameters followed by thresholding. A multi-pass algorithm with decreasing interrogation window size (64 x 64 to 32 x 32 pixels with 50% overlaps) was run to accomplish cross correlation computation on the instantaneous velocity vectors of the generated field. A post processing filter was then applied to vectors to remove outliers. In order to conduct spatial attenuation and flux calculations, velocity vectors were then exported as 80 x 64 cell grids (16 x 16 pixel cells with velocity in the (x,y) directions represented by (u,v)).

In order to better understand risk of detection by rheotactic predators, the spatial attenuation of flow (n) was calculated following Kiørboe *et al.* (2014) where

$$\| V_{flow} \| \propto r^n.$$

Flow speed was binned with variable thresholds of U^*, and r (magnitude of the spatial extent of flow) was defined as the radius of the circle of area equivalent to area demarcated by binned speed (U^*). To estimate attenuation of flow (n), a power law fitting was used, taking the slope of the regression.

To better understand how treatment affects feeding, the volume of fluid passing through a line segment (l) at maximum backwards velocity was initially calculated for five individuals. Later, the analysis was repeated across the whole stroke cycle. Body centroids calculated for previous analyses shifted location with amputation which consequently did not accurately match the location of the feeding region (labrum), and thus, a new adjusted centroid was calculated to standardize feeding region location between the two treatment groups. The adjusted centroid of the head shield (C') was defined as the center point between the landmarks of the horns and the posterior end of the head shield (P), the point at which the dts begins (Fig.1). The line segment for flux calculations was placed perpendicular to vector $\overrightarrow{C'P}$ and centered at three $\overrightarrow{C'P}$ away from C'. The length of the flux line corresponds to the approximate length of the head shield, which was defined as $2 \times \left|\overrightarrow{C'P}\right|$. 2D estimate of flux, ϕ, was calculated by summing the magnitude of velocity vectors projected onto the normal direction and then multiplying this value by velocity vector length

$$\phi_{x,y} = \sum(u, v) \cdot \hat{n}\, \mathrm{d}l.$$

$\hat{n}$ represents the normal unit vector, while the dot product provides the magnitude of velocity vector projected onto the normal direction. Relative flux in the frame of the nauplius's body was also calculated by subtracting naupliar velocity from absolute flux.

Dynamically Scaled Model and PIV

To analyze the difference in flow field around a larva with and without the dts, we towed a limbless dynamically-scaled model of the planktotrophic barnacle nauplius from the family *Lepadidae* through a tank of corn syrup to achieve a *Re* near unity (ranging from 1.5-3). Because of its long horns and spine, the model nauplius is similar in shape to that of our case study model genus *Octolasmis*. The model was constructed from 3D printed plastic using the software Rhino, and its unique construction allowed for body extensions (dts and frontal horns) to be added or removed interchangeably. Additionally, the model nauplius's center of mass was mounted to a force and moment transducer (data not included in this study) allowing the model to be towed easily from above using a robotic arm (sting). A small cart propelled using a stepper motor was rolled along the top of a clear acrylic tank (2.1 m length, 0.32 m width, 0.40 m depth) towing the model nauplius. When towed, the model nauplius was 13 cm from each wall minimizing possible wall effects.

The tank was seeded using neutrally buoyant 13 μm diameter, silver-coated, hollow glass spheres. Particles were illuminated from one side of the tank with a horizontal sheet of laser light produced by shining a 300mW, 532 nm laser through a prism. Videos of the model towed forward and backward with and without the dts were

then recorded with the model at various angles of attack (forward: 2° , backward: -9°) and at two different framerates (60 fps and 120 fps). Videos were then imported into DaVis (version 7) for flow field computation. Videos were cropped with manually implemented geometric masks. Model shape was masked using a combination of both algorithmic and manually implemented geometric masking methods. Cross correlation computation on instantaneous velocity vectors and vorticity was achieved using a multi-pass algorithm with interrogation window size of 24 x 24 pixels and weight of 8 x 8 pixels. Vector post-processing removed outlier vectors from the finalized vector fields. The presence of the sting disrupted flow, thus we quantified the flow field anterior and posterior to the sting separately. Flow fields from replicate tows were interpolated onto a shared grid and averaged in Matlab (Fig. 3).

Statistical Analysis

Statistical analyses were performed in R (version 3.6.2). For population scale analysis on free swimming nauplii, multiple videos of each treatment group accounted for replication, thus potential significance of video identity during video motion analysis was checked with a Linear Mixed Effect Model where treatment was categorized as a fixed effect and video identity (replication) as a random effect. Because video identity showed no significant effect on the analysis, this factor was then removed, and metrics of swimming were compared with a t-test. Normality and homogeneity of variance were checked with Q-Q plots and F-tests, respectively. Due to small sample size of kinematic, flow field, and dynamically scaled model observations, effect of amputation was tested with permutation F-tests (1000 Permutations).

Results

Behavior of population scale freely swimming larvae

Amputation resulted in significant effects on five of the seven tested metrics: Gross speed ($t_{1, 435} = 7.56$, $p < 0.001$), net speed ($t_{1, 435} = 6.03$, $p < 0.001$), net $V_{\text{free swim}}$ ($t_{1, 435} = -2.89$, $p = 0.004$), number of crossings ($t_{1, 435} = -4.27$, $p < 0.001$), and average crossing distance ($t_{1, 435} = 7.23$, $p < 0.001$, Fig. 2). Control group *O.cor* nauplii had 37.4% higher mean gross speed (observed difference: 0.2 mm s^{-1}) and 53.9% higher mean net speed (0.13 mm s^{-1}) than amputees. Net $V_{\text{free swim}}$ was -6.6% lower on average in control *O.cor* nauplii when compared to amputees. Crossings were significantly fewer and spaced further away in control *O. cor* which suggests overall less convoluted path trajectories (37.9 crossings in control compared to 58.3 crossings in amputees, 0.355 mm crossing distance in control compared to 0.229 mm in amputees).

Individual swimming kinematics

Amputated *O. warwickii* had decreased normalized speed by 26.2% when compared to the control group (Fig. 4, Table 1). Forward: backward displacement ratio, a measurement of stroke efficiency, was lower in amputees by 38.9%. An 8.8% lower limb beat frequency was also observed in amputated nauplii (Table 1). Both treatment groups operated in *Re* around one (1.83±0.45 and 0.74±0.37 for control and amputee, respectively). Significant differences in angular separation and phase lag were found across all but one time point and limb pair, with the exception of the start of the power stroke between antennule and antenna for both the left and right sides (Table 2).

Contralateral symmetry differences were observed between left and right mandible beat angle with 81.6% greater beat angle difference in amputees than controls during mid-power stroke (Fig. 4). Amputees beat their limbs at significantly greater amplitudes than controls for all appendages but the right-side antennule (Table 1). Additionally, amputees straightened both antennae at the end of the power stroke more than controls. The flexion angle of amputees' antennae at the end of the power stroke was >50% smaller than the control for both the left and the right sides (Table 1). Flexion ratio also differed significantly between treatments across multiple time points, with flexion occurring closer to the larval body among amputees (Fig. 5; Table 1).

Particle Image Velocimetry of live nauplii

Analysis of spatial attenuation displayed significant differences between amputees and control, but attenuation rates were within the same order of magnitude ($F_{1, 8} = 4.98$, $p = 0.005$, Fig. 6). The area of influence, i.e., area with flow velocity greater than the 80th percentile of all recorded velocity, were on average not different between the two treatment groups ($F_{1, 8} = 0.432$, $p = 0.5$). However, upon normalizing the samples by taking the square of body length, an approximate 3-fold larger fluid disturbance was observed in amputees (Fig. 6, $F_{1,8} = 12.4$, $p < 0.001$). Observed flux at the point of largest backward body velocity, displayed an average relative flux for amputees comparable to the control group ($F_{1, 8} = 1.35$, $p = 0.289$). However, the results were highly variable between individuals with standard deviations of 0.49 $mm^2\ s^{-1}$ for the control compared to 1.30 $mm^2\ s^{-1}$ for the amputated group (Fig. 6). Control nauplii had greater flux than

amputated nauplii when flux was integrated across the full limb beat cycle (Fig. 6, $F_{1, 8}$ = 5.73, p = 0.054).

Flow field around a dynamically scaled model

While flow fields looked comparable between the two treatment groups anterior to the sting, at the posterior end of the model, the magnitude of velocity vectors was larger and comprised a larger area when the spine was removed (Fig. 3). When the area with velocity exceeding the 80th percentile of all velocity vectors was delineated, a larger area of influence in amputees was not observed. The intact model (control) had an area of influence of 345 mm^2 and the model whose dts was removed (amputee) had an area of influence of 244 mm^2. However, when normalized by squared model length, amputated model results displayed a larger area of influence (0.023) when compared to controls (0.017), like flow field results of the individual-scale, free-swimming nauplius (Fig. 3).

Discussion

Many planktonic organisms, including highly mobile natatory forms, have long body extensions suggesting that these extensions likely have functions beyond anti-predation. To determine the possible functions, I investigated the biomechanical role of the dts of stage II barnacle nauplii from the genus *Octolasmis,* which possess extremely long spines and horns. My observations highlight the role of body extensions in enhancing swimming proficiency, reducing predation risk, and directing flow for feeding. Upon amputation, various potentially compensatory changes in limb kinematics were observed including increased stroke amplitude, increased limb-limb angular separation to

generate larger propulsive force, and reduced flexion angle at the beginning of the recovery stroke which may help with streamlining. While these compensatory kinematic changes may help to reduce the effects of amputation, they are not sufficient to eliminate all negative effects on swimming performance. These observations help to highlight how interactions between rigid morphological structures like spines interact with moving limbs to shape key ecological functions of multi-legged swimmers.

Reductions in spine length compromise swimming

Freely swimming amputated *O. cor* nauplii display lower net and gross speeds as well as higher numbers of crossings across the mid-line approximating smoothing spline indicating that paths are more convoluted and display sawtooth-like trajectories (Fig. 2). Similar results in high-speed videography of *O. warwickii* support observed swimming speed reduction when nauplii are amputated (Fig. 4). These observed differences between treatment groups were unlikely due to handling stress since both amputated and control nauplii were manipulated with a probe. These changes in speed and trajectories were likely associated with the change in limb kinematics discussed later.

Spine loss and/or reduction in total body length can increase predation risk in multiple ways. In nature, partial predation is one mechanism for reduction in spine length, similar to that of amputation in my experiment (Ohman 1984; Elliott & Tang 2011). A reduction in body length could relax the size-limitation on feeding by predators, and such a relationship is demonstrated with plasticity in spine lengths of *Daphnia* (Schlüter *et al.* 1987; Herzog *et al.* 2016). Amputated nauplii underwent a >400 μm

(~40% of body length) reduction in overall size likely putting them at greater risk to size limited predators. Another potential risk to damaged nauplii is inability to escape the suction current of predators through swimming (Costello & Colin 1994). The observed reduction in swimming speed likely further compromises nauplii's ability to escape. As an alternative strategy to escaping suction, some crustacean nauplii undertake diel vertical migration for predator avoidance. To successfully diel vertically migrate, nauplii must match speeds of light attenuation in the water column throughout the day (Richards *et al.* 1996; Bonicelli *et al.* 2016). Because of their slowed speed, amputated nauplii have a decreased ability to catch up with these rates of light attenuation. Finally, potential risk to rheotactic predation is influenced by the "visibility" of hydrodynamic signal (Strickler & Twombly 1975; Kiørboe *et al.* 2014). Larger hydrodynamic signal (area of influence) among amputated nauplii likely also increases predation risk (see later discussion). Overall, injury to spines could effectively strip nauplii of many important predator avoidance strategies, and likely negatively affect survivorship.

Potential compensatory changes in limb kinematics

Observed reductions in swimming performance were accompanied by several changes in limb kinematics. First, increases in limb beat amplitude were observed in amputees. In modeled crustacean swimming, increases in amplitude allowed for a trend of increasing net displacement per cycle until an eventual plateau due to interactions between neighboring limbs (Lenz *et al.* 2015; Takagi 2015). Second, the flexion angles of the antennae were smaller, i.e., limbs were straighter, among amputated nauplii at the end of the power stroke than in controls. I focused on the antennae because they are the main

propulsors, and the mandible activities of this species are highly modified and harder to quantify (Gauld 1959; Moyse 1984; Williams 1994). Swimming pteropods and nauplii of other crustaceans at comparable *Re* are observed to orient their limbs parallel to flow in order to minimize drag (Hessler 1985; Johnson & Tarling 2008). Similar to this behavior, reduction in flexion angle at the end of the power stroke may act to decrease drag and add to amputees' forward motion. Additionally, conserved bending kinematics across organisms in high *Re* placed the optimal range of maximum propulsor flexion angle at the beginning of the power stroke between 14.5°-38.4° (Lucas *et al.* 2014). Both control and amputated nauplii lie within this range with 19.5° for control and 25.6° for amputees. These two kinematic adjustments (increased beat amplitude and decreased curvature at the end of the power stroke) may act in conjunction to partially compensate for spine loss. However, it is important to note that with a $Re \approx 1$, streamlining during recovery stroke translates into further backward displacement causing amputees to be less efficient at swimming forward per stroke cycle.

A third difference between treatments was larger phase lag in amputees. Previous comparisons between planktotrophic and lecithotrophic barnacle nauplii suggested that anti-phase beating of the appendages acts as an anchor, tethering the larva in place to direct food particles towards the food capture area (Wong *et al.* 2020a). In Antarctic krill, increases in phase lag at intermediate *Re* resulted in wider gaps between neighboring appendages and reduced the total momentum of the propulsion jet due to dissipation of vortices (Ford *et al.* 2019). Similar increases of phase lag in copepods also lowered net displacement (Lenz *et al.* 2015). Here, phase lag between appendages increased significantly for amputees and likely reduced propulsive efficiency. Specifically, at the

start of the recovery stroke, greater phase lag exhibited by amputees resulted in limb-limb interactions between the antenna and mandible. Larger phase separation between neighboring limbs and interaction between the antenna and mandible may cause amputee nauplii to slip backward during the recovery stroke.

A final shift in kinematics was the adjustment in contralateral symmetry in which left and right pairs of appendages beat out of sync (Fig. 4, Table 1). In copepods, naupliar turning on the vertical axis (yaw) has been described to occur as a result of pronation or supination of the antenna such that one side drives more fluid motion than the other (Niimoto *et al.* 2020). Other mechanisms of turning at low *Re* have been observed such as lateral turning through asymmetrical limb beats across the vertical axis during the power stroke (Bruno *et al.* 2012). I observed a significant change in mandible symmetry during mid-power stroke in amputated nauplii, which likely resulted in turning over the vertical axis (yaw). For amputees, drag was reduced due to removal of the dts, and thus, a reduction in effective cross-sectional area. Furthermore their ability to maintain directed motion might have been further compromised due to adjustments in weight distribution, increasing torque experienced in moving water (Vogel 1981; Grünbaum & Strathmann 2003). In this case, the dts seems to act as a tether. The kinematic changes such as asymmetrical limb beat could be another form of partial compensation.

Spine loss changed fluid flow

Amputees had a larger normalized area of influence (Fig. 6). The risk of predation by rheotactic predators is proportional to hydrodynamic signal (Kiørboe *et al.* 2014).

Therefore, the loss of the spine in amputated nauplii likely increases predation risk. Observations of the dynamically scaled model support this conclusion. The higher normalized area of influence in live nauplii suggest limb kinematics and the interactions between limbs and body morphology had significant impact on fluid dynamics. Average spatial attenuation (*n*) of both groups of live nauplii was ~1 (Table 1), which is comparable to other planktonic nauplii (*Tetraclita japonica* and *Capitulum mitella*) (Wong *et al.* 2020a; Wong *et al.* 2020b). Compared to n of ~3 for the lecithotrophic *Polyascus planus*, the extreme length of the dts in *Octolasmis* likely does not aid in flow attenuation. Previous observations suggest maximum flux towards the labrum occurred during the recovery stroke (Wong et al., 2020a). However, at the point of largest backward velocity, relative flux remained comparable between the two treatment groups. When flux was integrated over the entire stroke cycle, a significantly larger relative flux was observed in the control group than amputees, suggesting more efficient feeding.

While body extensions of zooplankton have previously been characterized as structures useful in predator deterrence and buoyancy regulation, my observations imply that these structures likely have additional biomechanical roles. The dts interacts with flexible beating appendages to affect metrics such as swimming speed, trajectory, and hydrodynamic disturbance of an individual. As such, these body extensions play important biomechanical roles in planktonic organisms, and the constraints placed on the organisms by these body extensions likely have and will continue to influence the diversification of naupliar form.

Acknowledgements

I would like to thank my advisor Prof. Kit Yu Karen Chan for her nonstop support and guidance. I would also like to thank Veronica Chua, Moey Rojas, and the rest of the Chan lab for their time and effort in helping me develop my experiment's story. I am indebted to Daria Syskine for their keen eye for detail and checking my drafts for errors. I thank Shar Daniels, Ceci Williamson, Shaoni C. White, Ismail Can, and Isaac Satz for their personal support, which significantly includes providing me with food and snacks. Thank you, Lux Barton, for telling me to go to sleep. Finally, I would like to thank my parents who have supported me in innumerable ways during this process.

Table 1. Limb kinematics and hydrodynamic disturbance of control and amputated *Octolasmis warwickii* nauplii. PS: start of power stroke, MPS: mid-power stroke, RS: start of recovery stroke, MRS: mid-recovery stroke. Ant1: antennule, ant2: antennae, mand: mandible. Statistically significant differences ($p < 0.05$) are written in boldface.

			Control ($\bar{x}_c \pm$ SD)	**Amputated ($\bar{x}_a \pm$ SD)**	**F**	***p***
Speed (mm s^{-1})			**1.65±0.305**	**1.25±0.359**	**6.52**	**0.028**
Forward: backward displacement ratio			**3.81 ±1.72**	**2.33±1.31**	**4.52**	**0.045**
Beat frequency (Hz)			**2.53 ±0.128**	**2.31±0.123**	**15.1**	**0.004**
Asymmetry (°)	Ant1	PS:	0.879 °±8.07 °	-3.23°±25.6°	0.211	0.667
		MPS:	1.37 ° ±8.52 °	-0.518 ° ±19.8 °	0.0694	0.822
		RS:	1.34° ±6.43 °	-2.06 ° ±16.5 °	0.336	0.580
		MRS:	2.78 ° ±10.1 °	-4.82 ° ±13.9 °	1.81	0.197
	Ant2	PS:	-1.31 ° ±10.2 °	-6.19 ° ±17.7 °	0.520	0.467
		MPS:	0.900 ° ±15.6 °	-4.60 ° ±26.0 °	0.302	0.582
		RS:	1.44 ° ±11.0 °	4.63 ° ±16.6 °	0.238	0.613
		MRS:	-0.386 ° ±6.43 °	0.316 ° ±25.4 °	0.00670	0.939
	Mand	PS:	-4.17 ° ±11.1 °	0.582 ° ±14.9 °	0.615	0.448
		MPS:	**-6.56 ° ±12.7 °**	**5.36 ° ±10.8 °**	**4.87**	**0.035**
		RS:	-3.35 ° ±5.34 °	4.08 ° ±11.5 °	3.14	0.102
		MRS:	-3.28 ° ±10.4 °	3.58 ° ±8.37 °	2.54	0.144
Amplitude (°)	Left –ant1		**17.6°±6.16 °**	**36.8°±20.9 °**	**6.95**	**0.014**
	Left –ant2		**80.5°±10.2 °**	**93.5°±13.7 °**	**5.46**	**0.037**
	Left-mand		**17.5°±4.40 °**	**31.6°±11.4 °**	**12.2**	**0.002**
	Right-ant1		19.3°±5.54°	24.4°±13.7°	1.08	0.358
	Right-ant2		**80.6°±10.7°**	**95.3°±16.4°**	**5.25**	**0.045**
	Right-mand		**19.5°±6.83°**	**29.6°±7.29°**	**9.62**	**0.008**
Flexion angle (°)	Left – ant2	PS:	14.7°±11.6 °	23.2 °±11.5 °	2.54	0.117
		MPS:	31.6 °±32.3 °	48.2°±26.7°	1.50	0.225
		RS:	**108°±11.8°**	**51.0°±27.0°**	**34.3**	**0.001**
		MRS:	61.5°±42.7°	44.9°±26.7°	1.06	0.329
	Right –ant2	PS:	19.6°±14.4°	25.8°±9.26°	1.27	0.295
		MPS:	48.9°±41.3°	49.0°±23.3°	0.00	0.996
		RS:	**105°±19.4°**	**47.2°±20.2°**	**40.5**	**0.001**
		MRS:	61.4°±36.0°	45.4°±23.6°	1.34	0.258
Flexion ratio	Left – ant2	PS:	**0.837±0.071**	**0.730±0.114**	**5.88**	**0.019**
		MPS:	0.801±0.087	0.739±0.101	2.02	0.189
		RS:	0.652±0.047	0.691±0.092	1.33	0.244
		MRS:	**0.764±0.055**	**0.694±0.079**	**4.95**	**0.048**
	Right –ant2	PS:	**0.835 ±0.046**	**0.720±0.059**	**22.2**	**<0.001**
		MPS:	0.783±0.062	0.739±0.099	1.30	
		RS:	0.662±0.057	0.639±0.057	0.452	0.321
		MRS:	**0.792±0.045**	**0.699±0.083**	**8.91**	0.509
						0.008

Absolute area of influence (mm^2)	0.646±0.032	0.663±0.05	0.432	0.500
Body length^2 normalized area of influence	**0.621±0.07**	**2.05±0.90**	**4.98**	**0.005**
Spatial attenuation power (*n*)	**-1.17±0.040**	**-1.28±0.102**	**12.4**	**<0.001**
Relative flux ($mm^2\ s^{-1}$)	-1.39±0.439	0.495±1.49	1.35	0.289

Table 2. Angular separation for each combination of appendages at start of power stroke (PS), mid power stroke (MPS), start of recovery stroke (RS), and mid recovery stroke (MRS) for both treatment groups, control and amputated. These values were computed by subtracting the limb beat angle of the second limb listed from the first.

Appendage Pair	Time Point	Control ($\bar{x}_c \pm$ SD)	Amputated ($\bar{x}_a \pm$ SD)
Left antennule and antenna	MPS	40.2±16.8	68.2±29.1
	RS	82.2±3.65	104±17.5
	MRS	38.6±13.5	60.7±23.4
Right antennule and antenna	MPS	39.7±14.9	64.1±28.6
	RS	82.3±15.7	110±28.0
	MRS	35.4±13.8	65.9±25.0
Left antennule and mandible	PS	18.4±8.16	119±23.0
	MPS	16.8±9.01	117±25.1
	RS	18.7±5.15	100±23.1
	MRS	15.1±10.0	119±20.9
Right antennule and mandible	PS	13.4±6.59	122±25.6
	MPS	8.91±10.4	123±25.6
	RS	14.0±9.11	106±25.1
	MRS	9.03±9.48	128±15.8
Left antenna and mandible	PS	6.47±11.9	101±10.0
	MPS	-23.3±16.4	49.2±24.5
	RS	-63.5±5.85	-3.41±29.4
	MRS	-23.5±12.8	58.9±24.5
Right antenna and mandible	PS	3.60±6.71	108±12.2
	MPS	-30.8±13.1	59.2±22.7
	RS	-68.3±10.5	-3.98±23.1
	MRS	-26.4±14.1	62.1±15.3

Figure 1. Nauplii in the two treatment groups, (A) control and (B) amputated, marked with landmarks used for kinematics analysis; Fh, frontal horn; Dts, dorsal thoracic spine; XDts, amputated dorsal thoracic spine, P, posterior point on head shield, C′, head shield centroid. AP indicates the abdominal process. Black lines indicate vectors from body centroid to appendage tips ($\overrightarrow{CA}$) and body centroid to tip of the dorsal thoracic spine ($\overrightarrow{CP}$) for calculating limb angles, and vectors from centroid to point of maximum antenna curvature and curvature point to antenna tip for calculating flexion angle and ratio. Line for flux calculation is 3 $\left|\overrightarrow{C'P}\right|$ from C′.

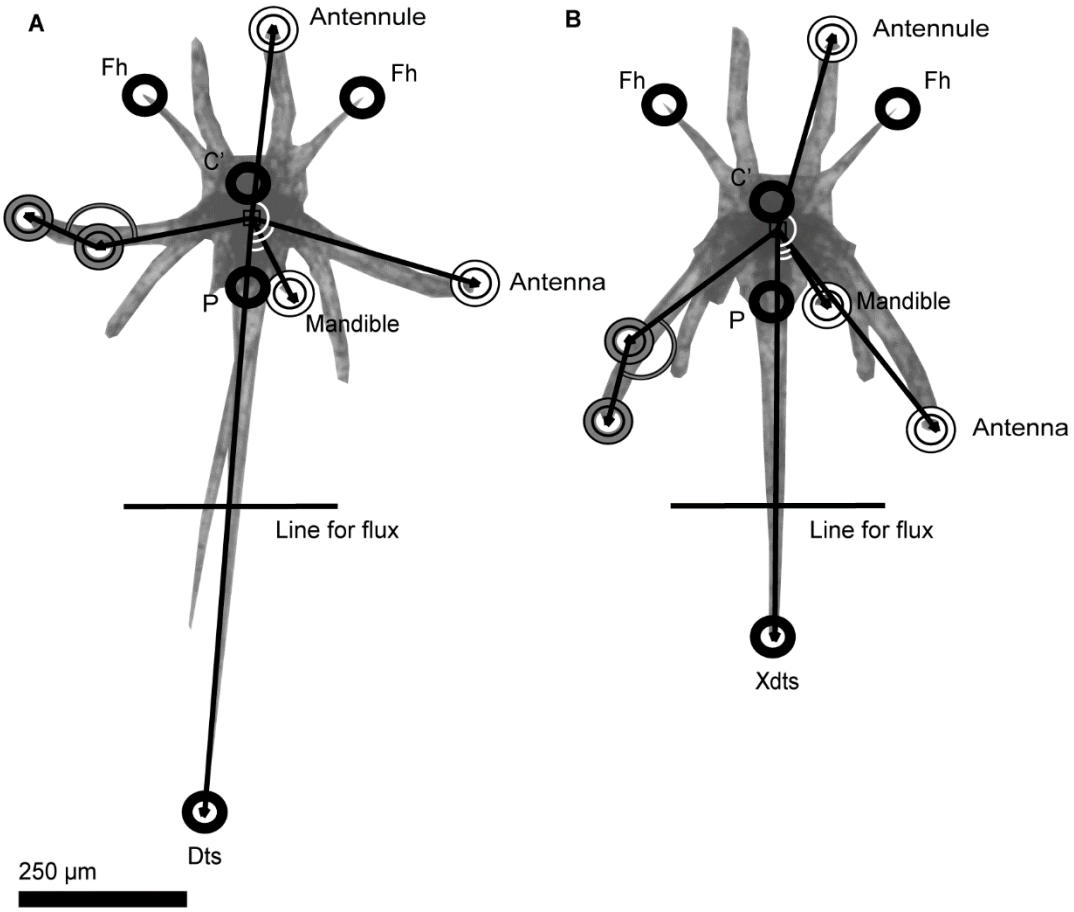

Figure 2. Population-level observation of freely swimming *Octolasmis cor* nauplii (A-F, 267 and 170 trajectories for control and amputees, respectively). All boxplots compare control treatment (white) with amputated treatment (grey). Each box represents the 1st and 3rd quartiles with maximum and minimum values represented by extended lines perpendicular to the box. Mean values are represented by the line within each box. $p < 0.001$ is marked by asterisks (***). Swimming trajectory in grey and smoothing spline along the midline in black and "crossings" are marked with black crosses (G). Representative example swimming trajectories of control (H) and amputated nauplii (I).

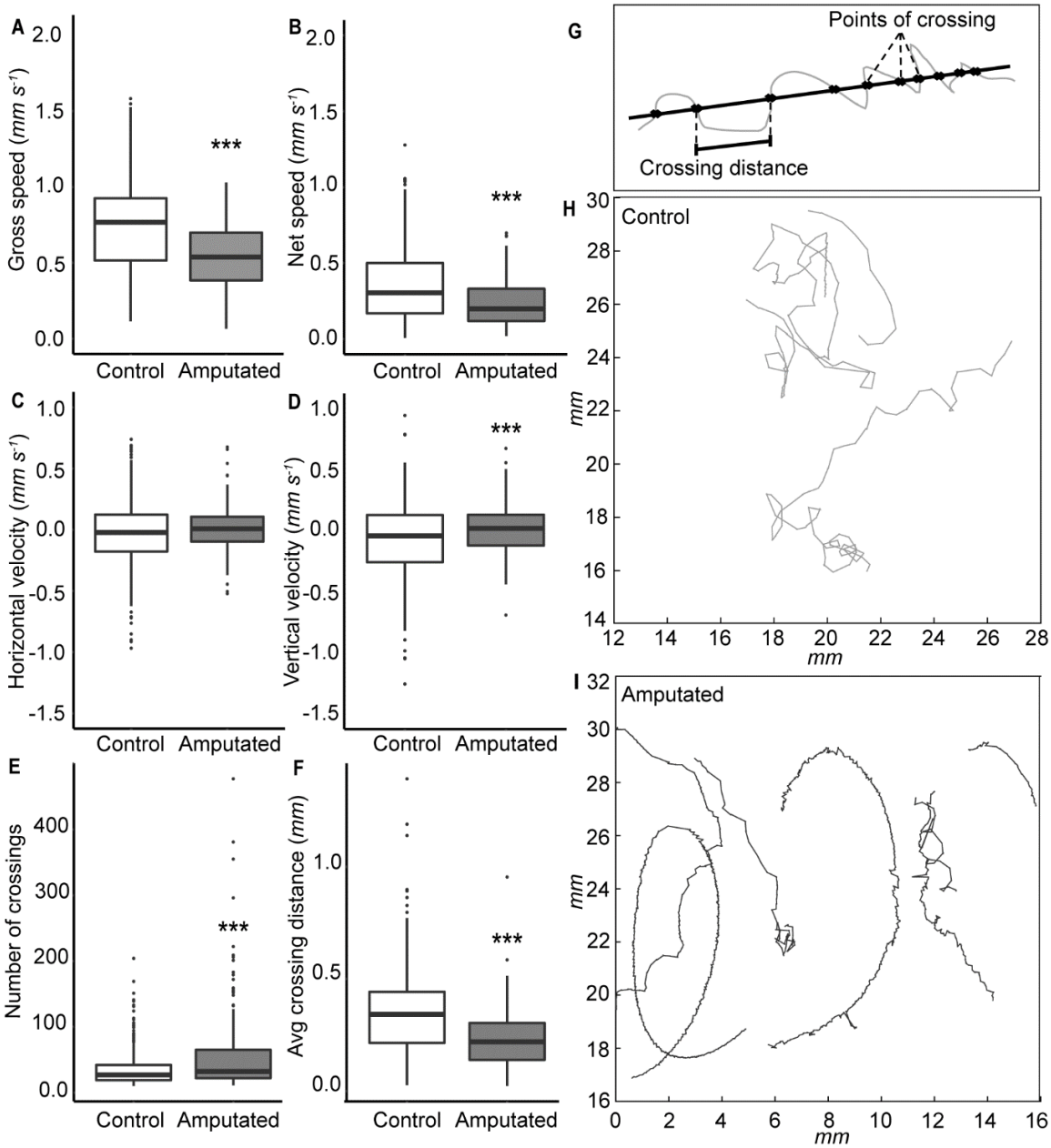

Figure 3. Dynamically scaled model of the two treatment groups (A) control and (B) amputated. Model body was masked with a combination of algorithmic and geometric masks. Both panels display generated velocity vectors (magnitude of black arrows) and velocity fields (blue to yellow gradient). X and Y axes measured in mm.

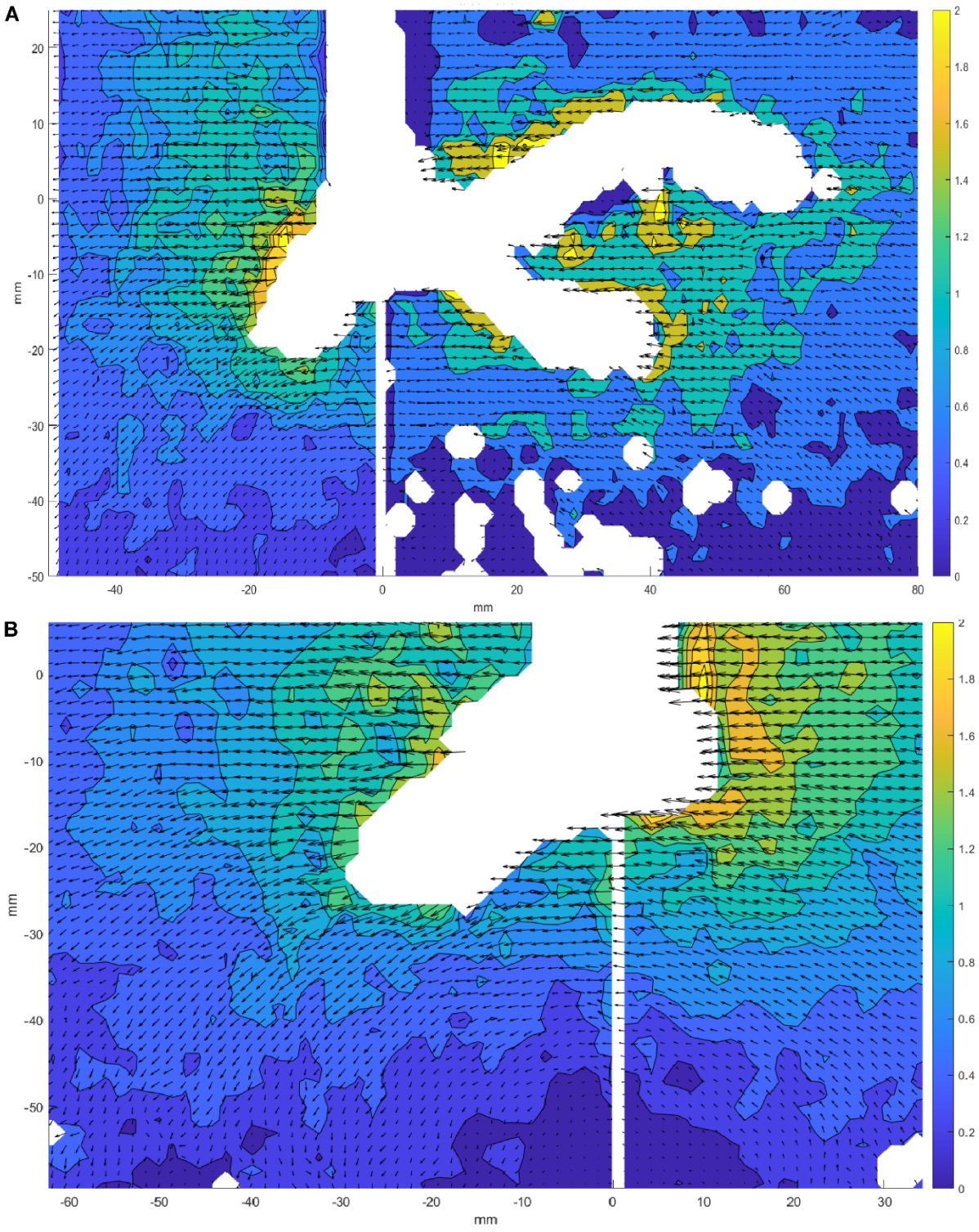

Figure 4. Limb angles of control (A, B) and amputated (D, E) *Octolasmis warwickii* nauplii through one limb beat cycle. All 3 pairs of appendages (ant1: antennule, ant2: antenna, mand: mandible) on both the left and right were tracked. Vertical light grey lines denote the start of the power stroke (PS), mid power stroke (MPS), start of recovery stroke (RS), and mid recovery stroke (MRS). Control larvae displayed higher net displacement (C, F) and forward: backward ratio compared to amputees (J). Amputated nauplii had larger limb beat angle (G) and angular separation between limb pairs (H); only data for the left side is shown. The largest difference in asymmetry between the left and right pairs of limbs is displayed for the mandible during mid power stroke (I). See Fig. 2 for details of boxplots. * indicates $p < 0.05$, ** indicates $p < 0.01$, *** indicates $p < 0.001$.

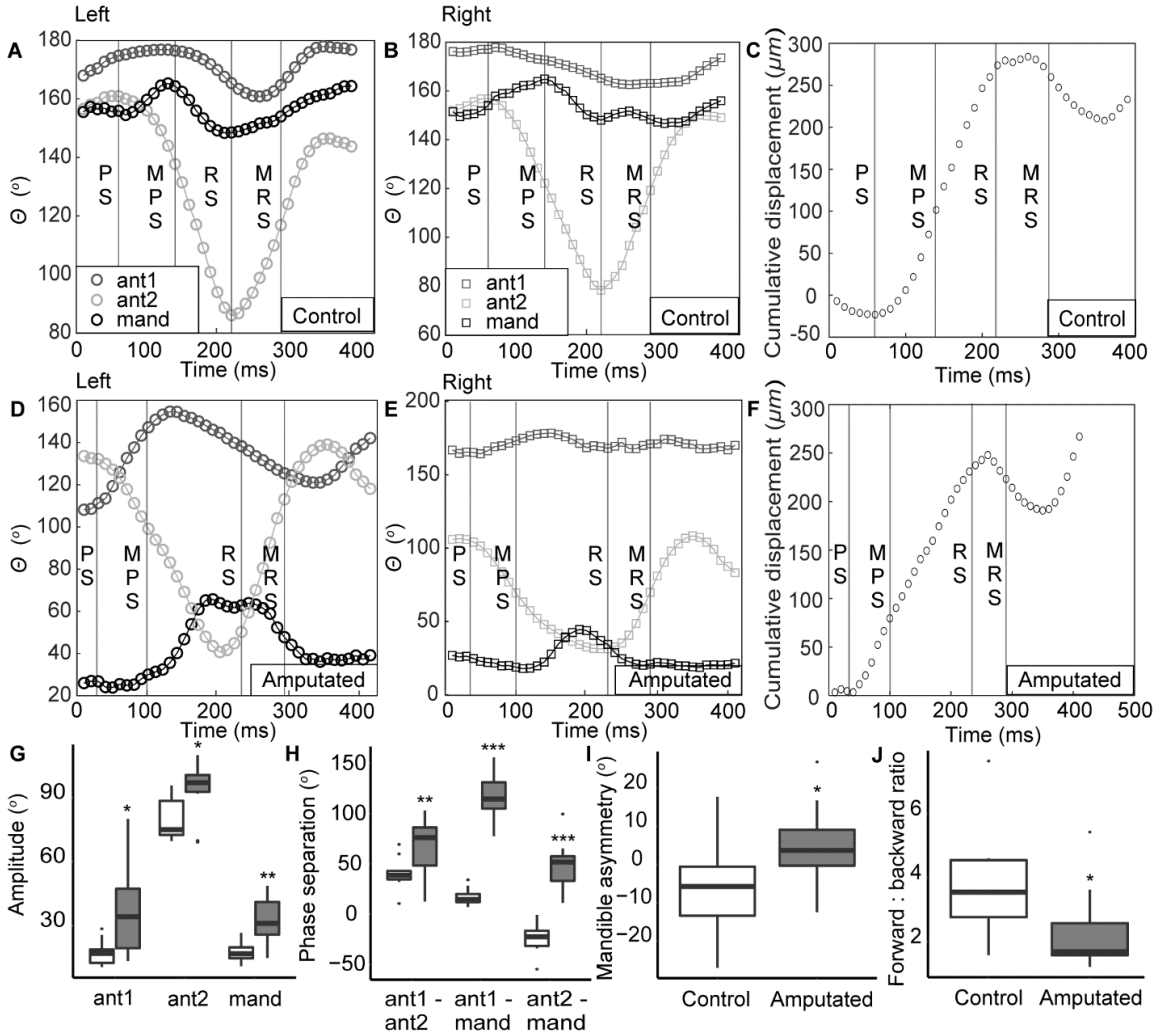

Figure 5. Flexion angle of the left antennule for control (A, E, I, M) and amputated *Octolasmis warwickii* nauplii (B, F, J, N) through a full limb beat cycle. Boxplots show the population mean (n = 9 for control and 10 for amputee) for flexion angle (C, G, K, O) and flexion ratio (D, H, L, P) at the corresponding time point of the stroke cycle. The four rows from the top to bottom correspond to the start of the power stroke (A-D), mid power stroke (E-H), start of the recovery stroke (I-L) and mid recovery stroke (M-P). Details of boxplots are given in figure 2. * denotes $p < 0.05$, *** denotes $p < 0.001$.

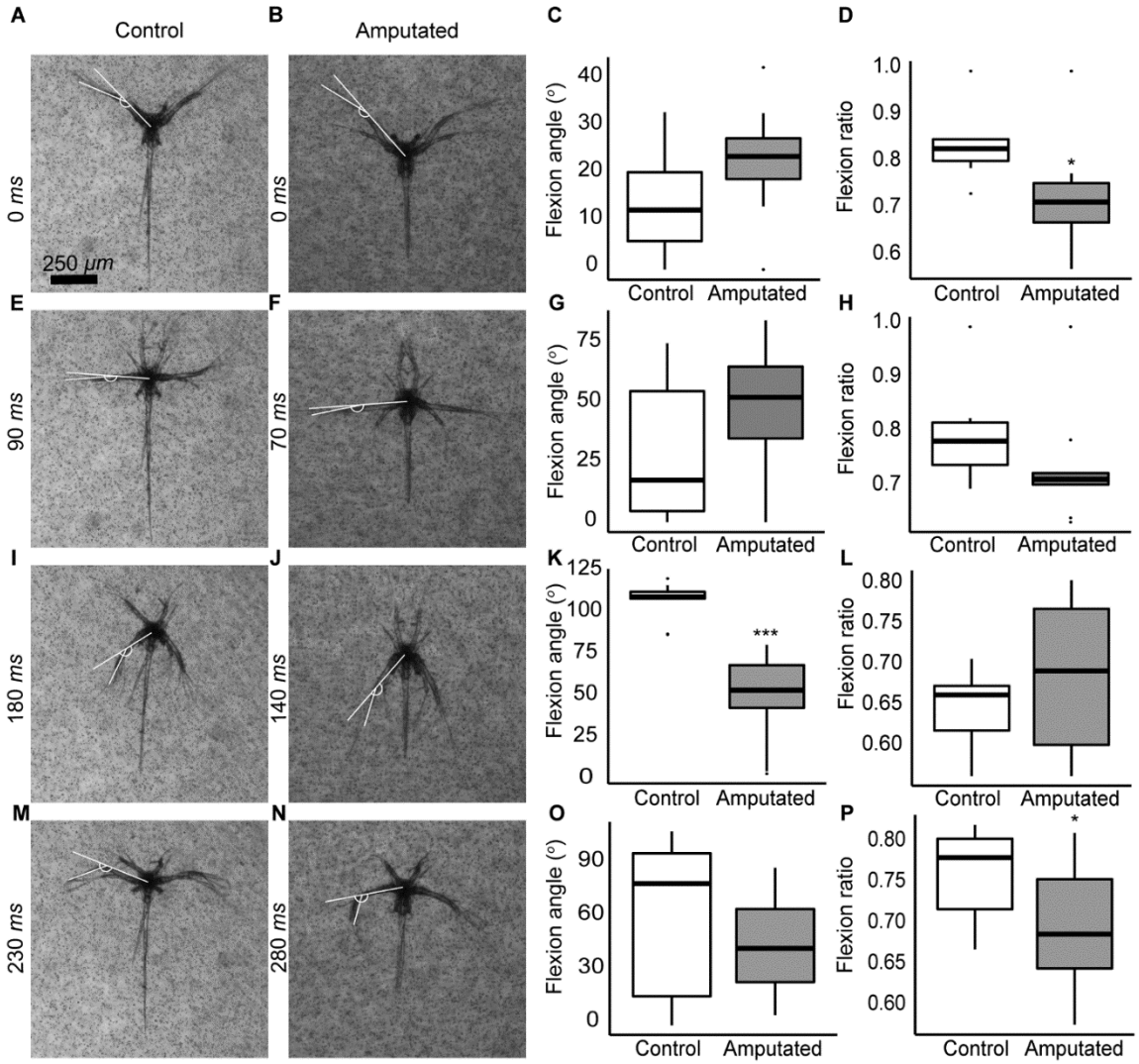

Figure 6. Flow field around representative *Octolasmis warwickii* nauplii with spine intact (A) and amputated (B) at the moment of maximum body backward displacement within the stroke cycle. Open squares mark the head shield centroid, open circles mark the midpoint of the flux line (black). The area of influence, normalized by squared body-length, was significantly higher in amputees (C). Initial analysis of relative flux was comparable between the two treatment groups when accounting for body velocity (D). However, after flux was integrated over a full limb beat cycle, control group nauplii were observed to have a significantly larger flux (E). * indicates $p < 0.05$, ** indicates $p < 0.01$.

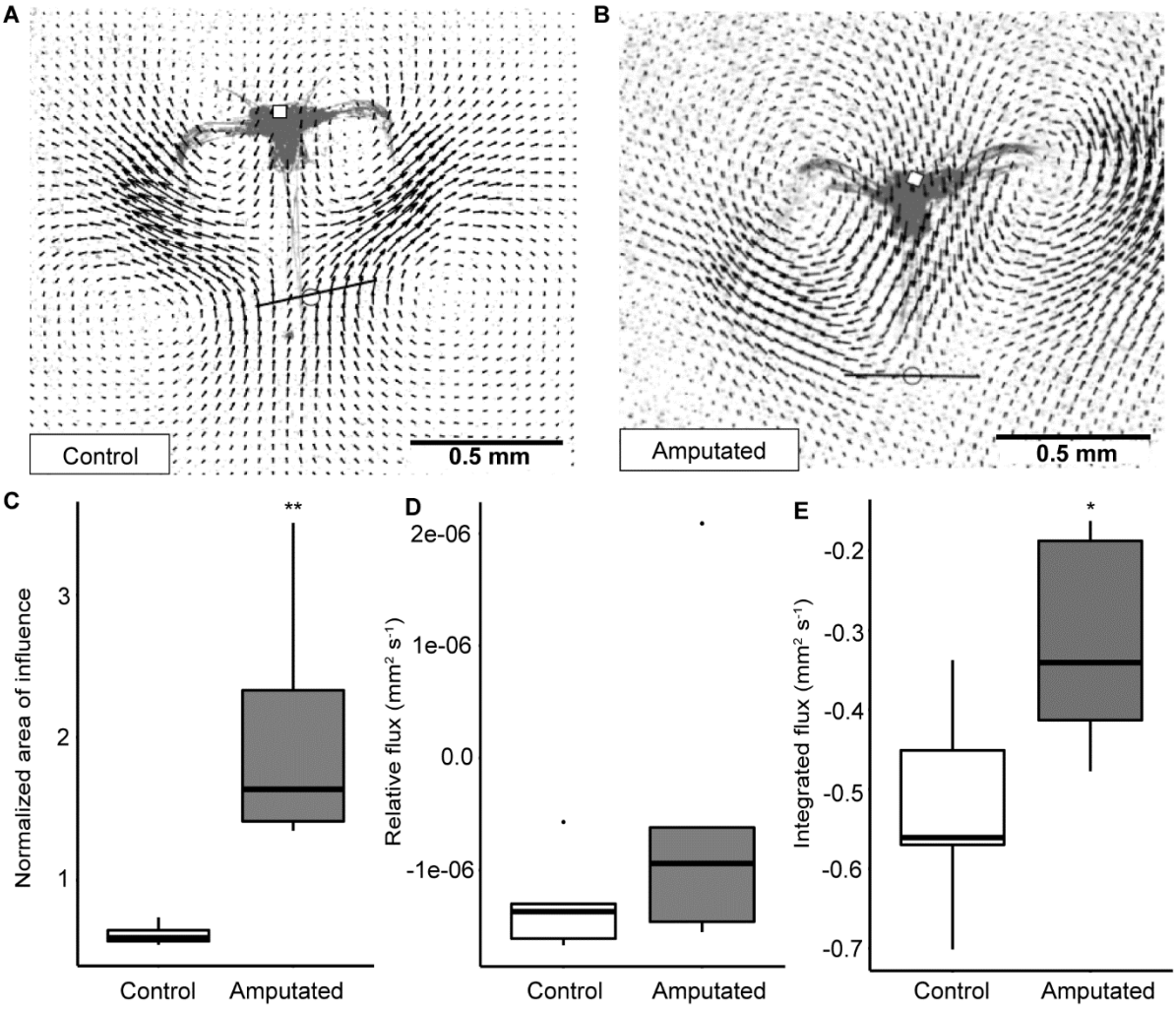

References

1.

Bonicelli, J., Tyburczy, J., Tapia, F.J., Finke, G.R., Parragué, M., Dudas, S. *et al.* (2016). Diel vertical migration and cross-shore distribution of barnacle and bivalve larvae in the central Chile inner-shelf. *Journal of Experimental Marine Biology and Ecology*, 485, 35-46.

2.

Bruno, E., Borg, C.M.A. & Kiørboe, T. (2012). Prey detection and prey capture in copepod nauplii. *PloS one*, 7, e47906.

3.

Chan, K.Y.K., Jiang, H. & Padilla, D.K. (2013). Swimming speed of larval snail does not correlate with size and ciliary beat frequency. *PloS one*, 8, e82764.

4.

Chew, L., Chong, V., Tanaka, K. & Sasekumar, A. (2012). Phytoplankton fuel the energy flow from zooplankton to small nekton in turbid mangrove waters. *Marine Ecology Progress Series*, 469, 7-24.

5.

Costello, J.H. & Colin, S. (1994). Morphology, fluid motion and predation by the scyphomedusa Aurelia aurita. *Marine Biology*, 121, 327-334.

6.

Dahms, H.-U. (2000). Phylogenetic implications of the crustacean nauplius. *Hydrobiologia*, 417, 91-99.

7.

Delcomyn, F. (1991). Perturbation of the motor system in freely walking cockroaches. I. Rear leg amputation and the timing of motor activity in leg muscles. *Journal of experimental Biology*, 156, 483-502.

8.

Elliott, D.T. & Tang, K.W. (2011). Spatial and temporal distributions of live and dead copepods in the lower Chesapeake Bay (Virginia, USA). *Estuaries and Coasts*, 34, 1039-1048.

9.

Emlet, R., Strathman, R. & Strickler, J. (1985). Gravity, drag, and feeding currents of small zooplankton. *Science*, 228, 1016-1017.

10.

Ford, M. & Santhanakrishnan, A. (2020). On the role of phase lag in multi-appendage metachronal swimming of euphausiids. *Bioinspiration & Biomimetics*.

11.

Ford, M.P., Lai, H.K., Samaee, M. & Santhanakrishnan, A. (2019). Hydrodynamics of metachronal paddling: effects of varying Reynolds number and phase lag. *Royal Society Open Science*, 6, 191387.

12.

Gauld, D. (1959). Swimming and feeding in crustacean larvae: the nauplius larva. In: *Proceedings of the Zoological Society of London*. Wiley Online Library, pp. 31-50.
13.

Gemmell, B.J., Jiang, H. & Buskey, E.J. (2014). A new approach to micro-scale particle image velocimetry (µPIV) for quantifying flows around free-swimming zooplankton. *Journal of plankton research*, 36, 1396-1401.
14.

Grünbaum, D. & Strathmann, R.R. (2003). Form, performance and trade-offs in swimming and stability of armed larvae. *Journal of Marine Research*, 61, 659-691.
15.

Gutarra, S., Moon, B.C., Rahman, I.A., Palmer, C., Lautenschlager, S., Brimacombe, A.J. *et al.* (2019). Effects of body plan evolution on the hydrodynamic drag and energy requirements of swimming in ichthyosaurs. *Proceedings of the Royal Society B*, 286, 20182786.
16.

Hayashi, R. & Takagi, D. (2020). Metachronal swimming with rigid arms near boundaries. *Fluids*, 5, 24.
17.

Herzog, Q., Tittgen, C. & Laforsch, C. (2016). Predator-specific reversibility of morphological defenses in Daphnia barbata. *Journal of Plankton Research*, 38, 771-780.
18.

Hessler, R.R. (1985). Swimming in crustacea. *Earth and Environmental Science Transactions of The Royal Society of Edinburgh*, 76, 115-122.
19.

Jiang, H. & Kiørboe, T. (2011). The fluid dynamics of swimming by jumping in copepods. *Journal of the Royal Society Interface*, 8, 1090-1103.
20.

Jiang, H., Meneveau, C. & Osborn, T.R. (2002a). The flow field around a freely swimming copepod in steady motion. Part II: Numerical simulation. *Journal of Plankton Research*, 24, 191-213.
21.

Jiang, H., Osborn, T.R. & Meneveau, C. (2002b). The flow field around a freely swimming copepod in steady motion. Part I: Theoretical analysis. *Journal of Plankton Research*, 24, 167-189.
22.

Johnson, M.L. & Tarling, G.A. (2008). Influence of individual state on swimming capacity and behaviour of Antarctic krill Euphausia superba. *Marine Ecology Progress Series*, 366, 99-110.
23.

Kiørboe, T., Jiang, H. & Colin, S.P. (2010). Danger of zooplankton feeding: the fluid signal generated by ambush-feeding copepods. *Proceedings of the Royal Society B: Biological Sciences*, 277, 3229-3237.
24.

Kiørboe, T., Jiang, H., Gonçalves, R.J., Nielsen, L.T. & Wadhwa, N. (2014). Flow disturbances generated by feeding and swimming zooplankton. *Proceedings of the National Academy of Sciences*, 111, 11738-11743.
25.

Koehl, M. (1998). Small-scale hydrodynamics of feeding appendages of marine animals. *Oceanography*, 11, 10-12.
26.

Koehl, M. (2003). Physical modelling in biomechanics. *Philosophical Transactions of the Royal Society of London. Series B: Biological Sciences*, 358, 1589-1596.
27.

Lamont, E.I. & Emlet, R.B. (2018). Permanently fused setules create unusual folding fans used for swimming in cyprid larvae of barnacles. *The Biological Bulletin*, 235, 185-194.
28.

Lenz, P.H., Takagi, D. & Hartline, D.K. (2015). Choreographed swimming of copepod nauplii. *Journal of The Royal Society Interface*, 12, 20150776.
29.

Lochhead, J.H. (1936). On the feeding mechanism of the nauplius of Balanus perforatus Bruguière. *Zoological Journal of the Linnean Society*, 39, 429-442.
30.

Loudon, C., Best, B. & Koehl, M. (1994). When does motion relative to neighboring surfaces alter the flow through arrays of hairs? *Journal of Experimental Biology*, 193, 233-254.
31.

Lucas, K.N., Johnson, N., Beaulieu, W.T., Cathcart, E., Tirrell, G., Colin, S.P. *et al.* (2014). Bending rules for animal propulsion. *Nature communications*, 5, 1-7.
32.

Martin, J.W., Olesen, J., Høeg, J.T. & Høeg, J. (2014). *Atlas of Crustacean Larvae*. JHU Press.
33.

Moyse, J. (1984). Some observations on the swimming and feeding of the nauplius larvae of Lepas pectinata (Cirripedia: Crustacea). *Zoological journal of the Linnean Society*, 80, 323-336.
34.

Murphy, D., Webster, D., Kawaguchi, S., King, R. & Yen, J. (2011). Metachronal swimming in Antarctic krill: Gait kinematics and system design. *Marine biology*, 158, 2541-2554.
35.

Niimoto, K., Kuball, K.J., Block, L.N., Lenz, P.H. & Takagi, D. (2020). Rotational Maneuvers of Copepod Nauplii at Low Reynolds Number. *Fluids*, 5, 78.
36.

Ohman, M.D. (1984). Omnivory by Euphausia pacifica: The role of copepod prey. *Marine ecology progress series. Oldendorf*, 19, 125-131.
37.

Padisák, J., Soróczki-Pintér, É. & Rezner, Z. (2003). Sinking properties of some phytoplankton shapes and the relation of form resistance to morphological diversity of plankton—an experimental study. In: *Aquatic biodiversity*. Springer, pp. 243-257.
38.

Purcell, E.M. (1977). Life at low Reynolds number. *American journal of physics*, 45, 3-11.
39.

Rainbow, P. & Walker, G. (1976). The feeding apparatus of the barnacle nauplius larva: a scanning electron microscope study. *Journal of the Marine Biological Association of the United Kingdom*, 56, 321-326.
40.

Richards, S.A., Possingham, H.P. & Noye, J. (1996). Diel vertical migration: modelling light-mediated mechanisms. *Journal of Plankton Research*, 18, 2199-2222.
41.

Schlüter, M., Groeneweg, J. & Soeder, C.J. (1987). Impact of rotifer grazing on population dynamics of green microalgae in high-rate ponds. *Water Research*, 21, 1293-1297.
42.

Strickler, J.R. (1998). Observing free-swimming copepods mating. *Philosophical Transactions of the Royal Society of London. Series B: Biological Sciences*, 353, 671-680.
43.

Strickler, J.R. & Twombly, S. (1975). Reynolds number, diapause, and predatory copepods: With 2 figures and 1 table in the text. *Internationale Vereinigung für theoretische und angewandte Limnologie: Verhandlungen*, 19, 2943-2950.
44.

Swadling, K., Ritz, D., Nicol, S., Osborn, J. & Gurney, L. (2005). Respiration rate and cost of swimming for Antarctic krill, Euphausia superba, in large groups in the laboratory. *Marine Biology*, 146, 1169-1175.
45.

Takagi, D. (2015). Swimming with stiff legs at low Reynolds number. *Physical Review E*, 92, 023020.
46.

Turner, J.T., Levinsen, H., Nielsen, T.G. & Hansen, B.W. (2001). Zooplankton feeding ecology: grazing on phytoplankton and predation on protozoans by copepod and barnacle nauplii in Disko Bay, West Greenland. *Marine Ecology Progress Series*, 221, 209-219.
47.

Vargas, C.A., ManrÍquez, P.H. & Navarrete, S.A. (2006). Feeding by larvae of intertidal invertebrates: assessing their position in pelagic food webs. *Ecology*, 87, 444-457.
48.

Vogel, S. (1981). *Life in Moving Fluids: The Physical Biology of Flow*. Willard Grant Press.

49.

Vogel, S. (1988). *Life's Devices: The Physical World of Animals and Plants*. Princeton University Press.

50.

Von Dassow, G. & Emlet, R.B. (2020). Direct observation of the setular web that fuses thoracopodal setae of a calanoid copepod into a collapsible fan. *The Biological Bulletin*, 238, 73-79.

51.

Walsby, A. & Xypolyta, A. (1977). The form resistance of chitan fibres attached to the cells of Thalassiosira fluviatilis Hustedt. *British Phycological Journal*, 12, 215-223.

52.

Williams, T.A. (1994). A model of rowing propulsion and the ontogeny of locomotion in Artemia larvae. *The Biological Bulletin*, 187, 164-173.

53.

Wong, J., Chan, B.K. & Chan, K. (2020a). Evolution of feeding shapes swimming kinematics of barnacle naupliar larvae: a comparison between trophic modes. *Integrative Organismal Biology*.

54.

Wong, J., Chan, B.K. & Chan, K.K. (2020b). Swimming kinematics and hydrodynamics of barnacle larvae throughout development. *Proceedings of the Royal Society B*, 287, 20201360.

55.

Wong, J., Chan, K.K. & Chan, B.K. (2018). Phylogenetic, ecological and biomechanical constraints on larval form: A comparative morphological analysis of barnacle nauplii. *PloS one*, 13, e0206973.

56.

Zhang, C., Guy, R.D., Mulloney, B., Zhang, Q. & Lewis, T.J. (2014). Neural mechanism of optimal limb coordination in crustacean swimming. *Proceedings of the National Academy of Sciences*, 111, 13840-13845.

57.

Zhang, Y., Zhang, J. & Ren, L. (2015). The terrestrial locomotion of a mole cricket with foreleg amputation. *Science China Technological Sciences*, 58, 999-1006.